JACS
JOURNAL OF THE AMERICAN CHEMICAL SOCIETY
Communication
pubs.acs.org/JACS

Dynamic Quantum Molecular Sieving Separation of D_2 from H_2–D_2 Mixture with Nanoporous Materials

Subaru Niimura,[†] Toshihiko Fujimori,[†] Daiki Minami,[†] Yoshiyuki Hattori,[‡] Lloyd Abrams,[§] Dave Corbin,[§] Kenji Hata,[∥] and Katsumi Kaneko*[,†]

[†]Research Center for Exotic Nanocarbons (JST), Shinshu University, 4-17-1 Wakasato, Nagano-city 380-8553, Japan

[‡]Faculty of Textile Science and Technology, Shinshu University, 3-15-1 Tokida, Ueda 386-8597, Japan

[§]DuPont Company CR&D, Experimental Station, Wilmington, Delaware 19880, United States

[∥]Research Center for Advanced Carbon Materials, National Institute of Advanced Industrial Science and Technology (AIST), 1-1-1 Higashi Tsukuba, Ibaraki 305-8565, Japan

Supporting Information

ABSTRACT: Quantum molecular sieving separability of D_2 from an H_2–D_2 mixture was measured at 77 K for activated carbon fiber, carbon molecular sieve, zeolite and single wall carbon nanotube using a flow method. The amount of adsorbed D_2 was evidently larger than H_2 for all samples. The maximum adsorption ratio difference between D_2 and H_2 was 40% for zeolite (MS13X), yielding a selectivity for D_2 with respect to H_2 of 3.05.

Deuterium is widely used in organic chemistry and biochemistry for isotopic labeling to elucidate the reaction mechanism.[1,2] Recently, the importance of substituting a hydrogen atom with a deuterium atom to improve the effectiveness of medicines has been shown in pharmaceutical technology.[3] Also, deuterium has contributed toward the analysis of materials in ^{2}H NMR[4,5] and neutron scattering studies.[6,7] Deuterium is a fuel for nuclear fusion[8] and demand for deuterium is anticipated to increase in the future. Separation of hydrogen isotopes can be carried out using the exchange reaction, thermal diffusion, distillation, adsorption, or the membrane method.[9−14] In particular, a combined electrolysis catalytic exchange method can be used to efficiently obtain a high separation factor, and is being actively studied.[15] However, many difficulties remain in the separation of deuterium and hydrogen.

Freeman indicated an essential contribution of quantum effect to a marked difference in H_2 and D_2 adsorption on charcoal at low temperature.[16] Beenakker et al. proposed a concept of quantum molecular sieving due to the quantum fluctuation difference in isotopes for separation of H_2 and D_2 using a cylindrical pore model.[17] Using quantum simulation, Johnson et al. predicted extremely high D_2 separation selectivity on the order of 10^2 for a H_2–D_2 mixture gas using single wall carbon nanotubes (SWCNT).[18−21] Tanaka et al. showed a quantum molecular sieving effect with single wall carbon nanohorns using a low temperature experiment and quantum simulation.[22] Equilibrium adsorption experiments using pure H_2 and D_2 showed explicitly that heavier D_2 molecules are adsorbed more in nanoscale pores than lighter H_2, and estimating the D_2 selectivity to be less than 10.[23] Further understanding of the quantum molecular sieving effect of nanoporous materials requires direct experimental information on the D_2 selectivity for the H_2–D_2 mixture.[23−25] Bhatia et al. showed theoretically the importance of the quantum molecular sieving effect in the adsorption kinetic process.[26,27] Recently, they showed the kinetic quantum effect on carbon molecular sieve with quasi-elastic neutron scattering for pure H_2 and D_2.[28] The kinetic quantum molecular sieving effect for the H_2–D_2 mixture should be studied experimentally, being helpful to design the separation process of D_2 from an H_2–D_2 mixture using the quantum molecular sieving effect.[29−31]

This letter describes the first report of the dynamic quantum molecular sieving selectivity of D_2 from an H_2–D_2 mixture on various nanoporous materials. We used a laboratory-designed flow-type mixed gas adsorption equipment consisting of a vacuum system, a mass filter, and flow controllers. Detailed information on the system is given in Figure S1. High purity H_2 (99.99999%) and D_2 (99.999%) were mixed to prepare the 1:1 mixed gas with flow control of H_2 and D_2. Activated carbon fiber (ACFs) having different pore widths, carbon molecular sieves (CMS5A), and SWCNTs were preheated at 423 K in vacuo for 4 h, and zeolites (MS4A, MS5A, MS13X, RHO and H-ZSM-11) were preheated at 573 K in vacuo for 8 h, respectively, before the kinetic adsorption measurement. The nanoporosity of the samples was determined by N_2 adsorption at 77 K. The nanopore structural parameters are given in Table 1.

The average pore width, w, is determined by the α_s-plot analysis for nanoporous carbon samples.[34] All of the adsorption isotherms of the samples used are given in Figures S2–S5. Time courses of the adsorbed H_2 and D_2 on the nanoporous samples were measured at 77 K after injection of the mixed gas (Figures S1 and S6). Here the test gas of the H_2–D_2 mixture of 500 Pa kept in the gas reservoir at 77 K was introduced into the adsorption cell and then the flow rate decreases from 0.25 to 0.006 mL (STP)/min during 5 min (average flow rate = 0.08 mL (STP)/min).

Figure 1 shows the time courses of the adsorption ratio of H_2 and D_2 on ACF20 and CMS5A. The adsorption ratio of H_2 or

Received: June 15, 2012
Published: November 1, 2012

   dx.doi.org/10.1021/ja305809u | J. Am. Chem. Soc. 2012, 134, 18483−18486

Table 1. Pore Structural Parameters

material	specific surface area (BET) (m^2 g^{-1})	specific surface area (α_s-analysis) (m^2 g^{-1})	pore volume (mL g^{-1})	w (nm)
ACF20	1660	1520	0.81	1.1
ACF15	1300	1250	0.60	1.0
ACF10	760	990	0.38	0.86
ACF7	640	1000	0.34	0.70
ACF5	520	830	0.27	0.65
CMS5A	390	610	0.20	0.67
MS4A	22	28	-	0.4[a]
MS5A	560	710	0.21	0.5[a]
MS13X	440	650	0.19	0.86[a]
RHO	630	920	0.31	0.48[a]
H-ZSM-11	350	430	0.17	0.65[a]
SWCNT-LA	330	320	0.15	1.0
SWCNT-SG	820	750	0.28	2.5

[a]The pore width values of zeolites are cited from the literature.[32,33]

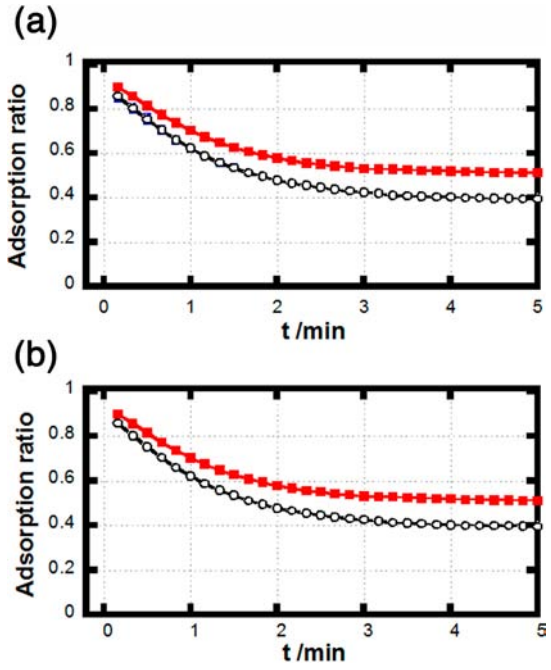

Figure 1. Time courses of the adsorption ratio of H_2 and D_2 on (a) ACF20 and (b) CMS5A. Black (opened) and red (filled) lines indicate H_2 and D_2, respectively.

D_2 was determined from the concentration change of each component of the injected mixed gas. The adsorption ratio is defined as the ratio of adsorption amount against total gas introduced; the adsorption amount was determined by the difference between total gas amount introduced and the not-adsorbed gas amount. Both D_2 and H_2 were adsorbed and their ratios decrease gradually, becoming almost constant after 3 min. As the pore size distribution of ACF and CMS5A is about less than ±15%, both of H_2 and D_2 are preferentially adsorbed in the smaller pores at the initial stage, giving rise to a decrease in the adsorption ratio with time. As the initial flow rate is the greatest and H_2 of a lighter molecule in the gas phase can arrive at the pore entrance earlier than D_2, restoration from overadsorption should occur more evidently in H_2 than D_2, decreasing the adsorption ratio with time. The adsorption ratio of D_2 is larger than that of H_2 for ACF20 and CMS5A; the adsorption discrepancy between D_2 and H_2 increases until 2 min, reaching a constant value of 12% difference for both samples.

To better understand the dynamic adsorption, we performed molecular dynamics (MD) simulations using the classical Lennard-Jones (LJ) potential and the quantum Feynman-Hibbs (FH) potential for verifying the classical diffusion effect and the quantum molecular sieving effect separately. Briefly, a mixture of H_2 and D_2 (1:1) was first randomly set outside the slit-shaped pores (w = 1.0 nm), and then performed the MD simulations. Details of our calculations are given in the Figure S7. Both the classical and quantum MD simulations reveal that lighter H_2 molecules adsorb on the pores faster than heavier D_2 molecules at the initial stage of dynamic adsorption (Figure S8). In the succeeding process, an adsorbed amount of D_2 exceeds that of H_2 in the quantum MD simulation, while difference in the adsorbed amounts is negligible in the classical MD simulation. This simulated result supports well the experimental results which show gradual enhancements of adsorption ratios between D_2 and H_2.

ACF20 and CMS5A have slightly distorted slit-shaped pores in which molecules can be accessible from different directions. On the other hand, zeolites have a pore network structure consisting of cylindrical shaped channels and thereby molecular accessibility is less favored than the slit-shaped nanoporous carbons. Figure 2 shows the time courses for the adsorption

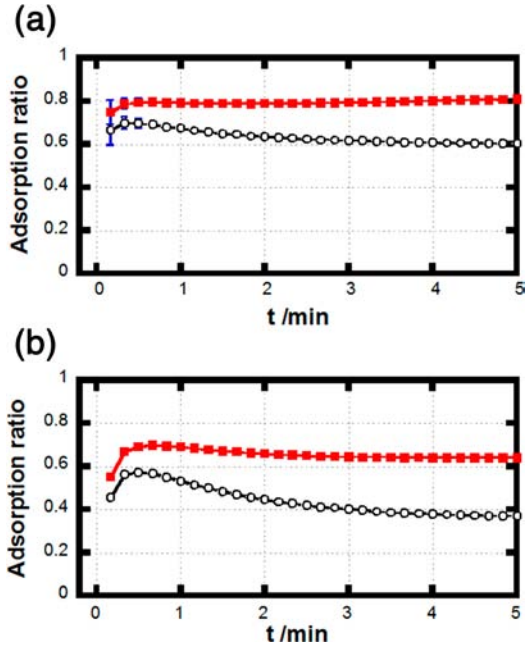

Figure 2. Time courses of the adsorption ratio of H_2 and D_2 on (a) MS4A and (b) MS13X. Black (opened) and red (filled) lines indicate H_2 and D_2, respectively.

ratio of H_2 and D_2 on MS4A and MS13X. The adsorption ratio of D_2 for both zeolites is almost constant, being larger than that of H_2. In contrast, the adsorption ratio of H_2 decreases gradually until 3 min, becoming almost constant as well as the carbon samples. The adsorption ratio differences between D_2 and H_2 are 25% and 40% for MS4A and MS13X, respectively.

This trend is rationalized by the classical MD simulation for the slit-shaped model with extremely narrow pores (w = 0.5

dx.doi.org/10.1021/ja305809u | J. Am. Chem. Soc. 2012, 134, 18483−18486

nm), which provide information on the accessibility of H_2 and D_2 into the pores (Figure S9). Because velocity of the lighter H_2 is much higher than that of the heavier D_2, a preferential adsorption of the H_2 molecules is confirmed by the classical MD simulations, implying the higher accessibility of the H_2 molecules. Though this entrance effect is further enhanced in the quantum MD simulations (Figure S10), adsorption of the quantum D_2 molecules turn out to be preferential as simulation time increases, due to the difference in the FH potentials for the H_2 and D_2 molecules. It indicates that classical diffusion into the pores is the primary factor in the initial stage, and the quantum effect becomes dominant in the succeeding adsorption stage. The entrance effect is suppressed in the wider pores, so that the dynamic adsorption is well described by the quantum effect at the entire simulation time (Figures S9–S11).

Other data for the time courses of the adsorption ratio of H_2 and D_2 are shown in Figures S12–S15. Here, the filling percent of pore spaces with hydrogen after 5 min is in the range of 0.6–4.1% (see Table S1) and the adsorption then proceeds in almost vacant pores.

These adsorption amounts and component concentrations in the gas phase for the D_2 and H_2 mixture provide the adsorption selectivity $S(D_2/H_2)$, as given by eq 1

$$S(D_2/H_2) = \frac{x_j/x_i}{y_j/y_i} \quad (1)$$

where, x and y indicate the adsorption amount and gas phase concentration for components i and j. Here, $i = H_2$ and $j = D_2$. Table 2 summarizes the $S(D_2/H_2)$ values for all nanoporous samples examined at 1 and 5 min.

Table 2. $S(D_2/H_2)$ at 1 and 5 min

	$S(D_2/H_2)$	
material	1 min	5 min
ACF20	1.49	1.61
ACF15	1.47	1.61
ACF10	1.50	1.66
ACF7	1.52	1.61
ACF5	1.58	1.61
CMS5A	1.53	1.60
MS4A	1.82	2.81
MS5A	1.87	2.59
MS13X	1.97	3.05
RHO	2.17	2.38
H-ZSM-11	1.80	1.77
SWCNT-LA	1.6	2.4
SWCNT-SG	1.7	2.0

The $S(D_2/H_2)$ value of all ACF samples and the carbon molecular sieve CMS5A after 1 and 5 min are 1.53 ± 0.05 and 1.61 ± 0.05, respectively, although ACF samples have the different pore widths ranging from 0.65 to 1.1 nm. These ACFs and CMS5A have slit shaped pores with sufficient accessibility for both D_2 and H_2 molecules to be rapidly adsorbed with less diffusion restriction by the preadsorbed molecules compared with cylindrical pores. The selectivity of ACF20, determined from the ideal adsorption solution theory using equilibrium adsorption isotherms of pure H_2 and D_2 on ACF20 at 20 K around 0.4 fractional filing in the previous study,[35] was 1.5, close to the observed value for the mixed gas experiment at 77 K. Therefore, H_2 and D_2 do not interact specifically. In contrast, zeolites have larger $S(D_2/H_2)$ values than nanoporous carbons. Also, zeolite samples, other than H-ZSM-11, show a time dependence of selectivity that is different from nanoporous carbons; the $S(D_2/H_2)$ value increases markedly from 1 to 5 min by 39–55% in the case of MS4A, MS5A, and MS13X. The selectivity of MS4A was measured at 131 and 300 K in addition to 77 K, as shown in Figures S16–18. The higher the temperature, the smaller the selectivity; the selectivity at 300 K was almost nil. This temperature dependence is characteristics of quantum molecular sieving.

As the zeolites used in this work have interconnected cylindrical pores giving rise to a more serious diffusion restriction, which can affect remarkably the dynamic quantum sieving effect, the zeolites should have high selectivity due to the kinetic quantum molecular sieving. The residual neck space after the preceding adsorption is more space-limited, and therefore, the succeeding adsorption depends more on the molecular size, inducing selective adsorption. Accordingly, zeolites are promising for the highly selective separation of D_2 from the H_2–D_2 mixture.

The selectivity of SWCNTs having straight and cylindrical pores is quite suggestive for the key factor for high selectivity. The $S(D_2/H_2)$ values for both SWCNTs at 1 min are intermediate between nanoporous carbons and zeolites. In particular, SWCNT-LA with pore width of 1.0 nm has a more remarkable increase in the $S(D_2/H_2)$ value than SWCNT-SG with pore width of 2.5 nm. The effective pore width of the SWCNT-LA is 1.0 nm, similar to that of MS13X. The entrance effect results in an increase in the $S(D_2/H_2)$ value with time, as mentioned above, even though the filling percent of the pores with hydrogen is less than 5%. The entrance effect in the one-dimensional pores in SWCNTs should be too intensive to suppress even the diffusion of D_2. As zeolites have interconnected pores, an appropriate diffusion with high selectivity can be guaranteed.

The dynamic D_2 selectivity due to quantum molecular sieving is thus evidenced by the H_2–D_2 mixed gas experiments using nanoporous carbons, zeolites, and SWCNTs; the promising pore structures for the high D_2 selectivity are interconnected cylindrical pores.

■ ASSOCIATED CONTENT

Supporting Information

Experimental procedures, details of MD simulations, and additional figures. This material is available free of charge via the Internet at http://pubs.acs.org.

■ AUTHOR INFORMATION

Corresponding Author

kkaneko@shinshu-u.ac.jp

Notes

The authors declare no competing financial interest.

■ ACKNOWLEDGMENTS

This study was carried out by the fund of the Strategic Promotion Program for Basic Nuclear Research by MEXT, Japan. We thank Micromeritics Instrument Corporation for partial support of the adsorption measurements. K.K., D.M., and T.F. were supported by Exotic Nanocarbons, Japan Regional Innovation Strategy Program by the Excellence, JST.

REFERENCES

(1) Miller, K. L.; Williams, B. N.; Benitez, D.; Carver, C. T.; Ogilby, K. R.; Tkatchouk, E.; Goddard, W. A., III; Diaconescu, P. L. *J. Am. Chem. Soc.* **2010**, *132*, 342−355.
(2) Gomez-Gallego, M.; Sierra, M. A. *Chem. Rev.* **2011**, *111*, 4857−4963.
(3) Sanderson, K. *Nature* **2009**, *458*, 269.
(4) Gall, C. M.; DiVardi, J. A.; Opella, S. J. *J. Am. Chem. Soc.* **1981**, *103*, 5039−5043.
(5) Tamura, A.; Matsushima, M.; Naito, A.; Kojima, S.; Miura, K.; Akasaka, K. *Protein Sci.* **1996**, *5*, 127−139.
(6) Schurtenberger, P.; Egelhaaf, S. U.; Hindges, R.; Maga, G.; Jonsson, Z. O.; May, R. P.; Glatter, O.; Hubscher, U. *J. Mol. Biol.* **1998**, *275* (1), 123−132.
(7) Rosi, N. L.; Eckert, J.; Eddaoudi, M.; Vodak, D. T.; Kim, J.; O'Keeffe, M.; Yaghi, O. M. *Science* **2003**, *300*, 1127−1129.
(8) Glugla, M.; Lasser, R.; Dorr, l.; Murdoch, D. K.; Haange, R.; Yoshida, H. *Fusion Eng. Des.* **2003**, *69*, 39−43.
(9) Miller, A. I. *Int. J. Hydrogen Energy* **1984**, *9* (1/2), 73−79.
(10) Yeh, H.-M.; Yang, S.-C. *Chem. Eng. Sci.* **1984**, *39* (7), 1277−1282.
(11) Bartlit, J. R.; Sherman, R. H.; Stutz, R. A.; Denton, W. H. *Cryogenics* **1979**, *19*, 275−279.
(12) Kotoh, K.; Nishikawa, T.; Kashio, Y. *J. Nucl. Sci. Technol.* **2002**, *39*, 435−441.
(13) Matsuyama, M.; Miyake, H.; Ashida, K.; Watanabe, K. *J. Nucl. Mater.* **1982**, *110*, 296−300.
(14) Chu, X.-Z.; Zhou, Y.-P.; Zhang, Y.-Z.; Su, W.; Sun, Y.; Zhou, L. *J. Phys. Chem. B* **2006**, *110*, 22596−22600.
(15) Sugiyama, T.; Asakura, Y.; Uda, T.; Shiozaki, T.; Enokida, Y.; Yamamoto, I. *Fusion Eng. Des.* **2006**, *81*, 833−838.
(16) Freeman, M. P. *J. Phys. Chem.* **1960**, *64*, 32−37.
(17) Beenakker, J. J. M.; Borman, V. D.; Krylov, A. Y. *Chem. Phys. Lett.* **1995**, *232*, 379−382.
(18) Wang, Q.; Challa, S.; Sholl, D. S.; Johnson, K. *Phys. Rev. Lett.* **1999**, *82* (5), 956−959.
(19) Challa, S. R.; Sholl, D. S.; Johnson, J. K. *Phys. Rev. B* **2001**, *63* (24), 245419.
(20) Garberoglio, G.; DeKlavon, M. M.; Johnson, J. K. *J. Phys. Chem. B* **2006**, *110*, 1733−1741.
(21) Garberoglio., G.; Johnson, J. K. *ACS Nano* **2010**, *4* (3), 1703−1715.
(22) Tanaka, H.; Kanoh, H.; Yudasaka, M.; Iijima, S.; Kaneko, K. *J. Am. Chem. Soc.* **2005**, *127*, 7511−7516.
(23) Noguchi, D.; Tanaka, H.; Fujimori, T.; Kagita, H.; Hattori, Y.; Honda, H.; Urita, K.; Utsumi, S.; Wang, Z.-M.; Ohba, T.; Kanoh, H.; Hata, K.; Kaneko, K. *J. Phys.: Condens. Matter* **2010**, *22*, 334207.
(24) Noguchi, D.; Tanaka, H.; Kondo, A.; Kajiro, H.; Noguchi, H.; Ohba, T.; Kanoh, H.; Kaneko, K. *J. Am. Chem. Soc.* **2008**, *130*, 6367−6372.
(25) Tanaka, H.; Noguchi, D.; Yuzawa, A.; Kodaira, T.; Kanoh, H.; Kaneko, K. *J. Low Temp. Phys.* **2009**, *157*, 352−373.
(26) Kumar, A. V. A.; Bhatia, S. K. *Phys. Rev. Lett.* **2005**, *95*, 245901.
(27) Kumar, A. V. A.; Jobic, H.; Bhatia, S. K. *J. Phys. Chem. B* **2006**, *10*, 16666−16671.
(28) Nguyen, T. X.; Jobic, H.; Bhatia, S. K. *Phys. Rev. Lett.* **2010**, *105*, 085901.
(29) Zhao, X.; Villar-Rodil, S.; Fletcher, A. J.; Thomas, K. M. *J. Phys. Chem. B* **2006**, *110*, 9947−9955.
(30) Chen, B.; Zhao, X.; Putkham, A.; Hong, K.; Lobkovsky, E. B.; Hurtado, E. J.; Fletcher, A. J.; Thomas, K. M. *J. Am. Chem. Soc.* **2008**, *130*, 6411−6423.
(31) Chu, X.-Z.; Zhou, Y.-P.; Zhang, Y.-Z.; Su, W.; Sun, Y.; Zhou, L. *J. Phys. Chem. B* **2006**, *110*, 22596−22600.
(32) Herron, N; Corbin, D. R., Eds. *Inclusion Chemistry with Zeolites: Nanoscale Materials by Design, Topics in Inclusion Science*; Kluwer Academic Publishers: London, 1995; p 7.
(33) Szostak, R. *Handbook of Molecular Sieves*; Van Nostrand Reinhold: New York, 1984; p 258.
(34) Kaneko, K.; Ishii, C. *Colloids Surf.* **1992**, *67*, 203−212.
(35) Hattori, Y.; Tanaka, H.; Okino, F.; Touhara, H.; Nakahigashi, Y.; Utsumi, S.; Kanoh, H.; Kaneko, K. *J. Phys. Chem. B* **2006**, *110*, 9764−9767.